



## Article

# Polymeric Nanocomposites of Iron–Oxide Nanoparticles (IONPs) Synthesized Using *Terminalia chebula* Leaf Extract for Enhanced Adsorption of Arsenic(V) from Water

Sadia Saif <sup>1,2,3,\*</sup> , Arifa Tahir <sup>2</sup>, Tayyaba Asim <sup>2</sup>, Yongsheng Chen <sup>1</sup> and Syed Farooq Adil <sup>4,\*</sup> 

<sup>1</sup> School of Civil and Environmental Engineering, Georgia Institute of Technology, Atlanta, GA 30332, USA; yongsheng.chen@ce.gatech.edu

<sup>2</sup> Department of Environmental Science, Lahore College for Women University, Lahore 54000, Pakistan; arifa.tahir@gmail.com (A.T.); tayyabasim2008@gmail.com (T.A.)

<sup>3</sup> Department of Environmental Sciences, Kinnaird College for Women, Lahore 54000, Pakistan

<sup>4</sup> Department of Chemistry, College of Science, King Saud University, P.O. Box 2455, Riyadh 11451, Kingdom of Saudi Arabia

\* Correspondence: sadia.saifpk@gmail.com or sadia.saif@kinnaird.edu.pk (S.S.); sfadil@ksu.edu.sa (S.F.A.); Tel.: +92-332-4543310 (S.S.)

Received: 18 October 2018; Accepted: 7 January 2019; Published: 27 January 2019



**Abstract:** This study demonstrates the ecofriendly synthesis of iron–oxide nanoparticles (IONPs) and their stabilization with polymers, i.e., chitosan (C) and polyvinyl alcohol (PVA)–alginate (PA), along with a further investigation for the removal of arsenic(As(V)) from water. IONPs with an average diameter of less than 100 nm were prepared via a green synthesis process using an aqueous leaf extract of *Terminalia chebula*. Batch experiments were conducted to compare the removal efficiency of As(V) by these adsorbents. Factors such as pH and adsorbent dosages significantly affected the removal of arsenate As(V) by IONPs and polymer-supported reactive IONPs. Several adsorption kinetic models, such as pseudo first-order, and pseudo second-order Langmuir and Freundlich isotherms, were used to describe the adsorption of As(V). The removal of As(V) by IONPs follows the Langmuir adsorption isotherm. The highest monolayer saturation adsorption capacity as obtained from the Langmuir adsorption isotherm for IONPs was 28.57 mg/g. As(V) adsorption by polymer-supported IONPs best fit the Freundlich model, and maximum adsorption capacities of 34.4 mg/g and 40.3 mg/g were achieved for chitosan- and PVA–alginate-supported IONPs, respectively. However, among these adsorbents, PVA–alginate-supported IONPs were found to be more effective than the other adsorbents in terms of adsorption, stability, and reusability.

**Keywords:** iron–oxide nanoparticles; green synthesis; polymer; chitosan; PVA–alginate; nanocomposite; arsenic

## 1. Introduction

Ensuring safe drinking water for the protection of human health is a challenge for the entire world. Due to rising industrialization, there are numerous pollutants that enter drinking water sources, such as As, Cd, Cr, Cu, Zn, Pb, Hg, and Ni [1,2]. Among the many pollutants, arsenic poses serious health risks and is considered a toxic pollutant when found in drinking water [3,4]. The predominant forms of arsenic in drinking water are its inorganic forms: Arsenite (As(III)) ( $\text{H}_2\text{AsO}_3^-$  and  $\text{H}_2\text{AsO}_3^{3-}$ ) and arsenate (As(V)) ( $\text{H}_2\text{AsO}_4^{4-}$  and  $\text{HAsO}_4^{2-}$ ) [5]. In order to make water drinkable, many conventional procedures were developed for the removal of arsenic from drinking water, such as oxidation [6], electrocoagulation [7], and adsorption of arsenic on activated mud [8] and activated carbon [9].

Among the various water treatment technologies, adsorption seems to be a more convenient and effective method for the removal of heavy metals in terms of cost and simplicity of process [10]. Iron and related adsorbents are popular for the remediation of water pollutants [11]. The intervention of nanotechnology opened a new horizon in the field of water purification [12]. Iron nanoparticles (NPs), which possess a high surface area and surface reactivity, are effectively used for water treatment [13,14]. Zero-valent iron nanoparticles (nZVIs) and iron oxide nanoparticles, such as  $\text{Fe}_2\text{O}_3$  and  $\text{Fe}_3\text{O}_4$  NPs, are among those commonly employed for the remediation of environmental pollution, particularly for the decontamination of water [15–18]. Magnetic nanoparticles and modified magnetic nanoparticles were found to be very effective for the removal of arsenic because of their strong adsorption activities, and they can be easily separated by employing an external magnetic field [19–21]. Evidence of the particle size influence on the ability to remove (adsorb) arsenic from water was observed, as smaller nanoparticles were found to exhibit more adsorption capacity and faster kinetics due to their higher specific surface area, shorter intraparticle diffusion distance, and larger number of surface reaction sites of nanoparticles [22,23]. The nanopowder form of metal oxides/hydroxides provides a high surface area for increased adsorption capacity; however, this small particle size also drives the need for energy-intensive post-treatment filtration to recover the nanoparticles for regeneration and reuse [24]. To overcome this issue, researchers focus on the immobilization and stabilization of nanoparticles.

The immobilization or stabilization of nanoparticles on solid supports has many advantages. The use of biopolymers gained wide attention due to their low cost and high content of amino and hydroxyl functional groups, which show significant adsorption potential for the removal of various heavy-metal ions [25,26]. Iron-coated polymeric materials and numerous biopolymers incorporated with nanoparticles were used to remove arsenic from water [27–29]. In this perspective, alginate and chitosan incorporated with magnetic iron nanoparticles proved very effective in the removal of toxic heavy metals from water [24,30,31].

Several methods are used to synthesize iron-oxide nanoparticles (IONPs) [32,33]. In recent times, the focus is directed toward eco-friendly synthesis of IONPs. Plant-based synthesis of IONPs using various plants such as leaf extracts of green tea [34], eucalyptus [35], pomegranate [36], guava [37], and grape [38] proved to be environmentally friendly alternative cost-effective solutions to some of the most challenging environmental clean-up problems. Furthermore, IONPs from the plant-mediated synthesis of IONPs were successfully used to solve other ecological problems, such as assisting in the removal of environmental pollutants, including organic pollutants [39], heavy metals [40,41], bacterial pathogens [42,43], dyes [44,45], and wastewater treatment [46].

Herein, we report an ecofriendly and nonhazardous green route for synthesizing  $\text{Fe}/\text{Fe}_2\text{O}_3$  nanoparticles using an aqueous extract of *Terminalia chebula*, which was reportedly found to contain polyphenols (punicalin, punicalagin, and terflavins B, C, and D) [47,48]. The obtained IONPs were stabilized using nontoxic natural polymers, i.e., chitosan and polyvinyl alcohol (PVA)–alginate to avoid aggregation and enhance the adsorption properties of nanoparticles for the removal of  $\text{As(V)}$ , a highly toxic inorganic element. For the adsorption studies of  $\text{As(V)}$  employing the green synthesized IONPs, batch experiments were conducted with varying conditions, such as pH, time, adsorbent dosages, and arsenic initial concentration. The adsorption isotherms and kinetics for  $\text{As(V)}$  removal were also studied. The reusability of adsorbents, i.e., iron nanoparticles and polymer nanocomposites, was explored; moreover, the release of ions from iron adsorbents was also measured.

## 2. Materials and Methods

### 2.1. Chemicals

All chemicals were purchased from Sigma Aldrich and included iron chloride ( $\text{FeCl}_3$ ) (anhydrous, powder,  $\geq 99.99\%$  trace metals basis), chitosan (medium molecular weight), polyvinyl alcohol (PVA), sodium alginate, sodium arsenate dibasic heptahydrate ( $\text{Na}_2\text{HAsO}_4 \cdot 7\text{H}_2\text{O}$ ), sodium hydroxide ( $\text{NaOH}$ ), boric acid ( $\text{H}_3\text{BO}_3$ ), calcium chloride ( $\text{CaCl}_2$ ), and nitric acid 69% ( $\text{HNO}_3$ ). Arsenic and iron metal standards (1000  $\mu\text{g/mL}$  in 2%  $\text{HNO}_3$ ) were purchased from High-Purity Standards, USA.

Fresh leaves of *Terminalia chebula* were collected from Bagh-e-Jinnah, Lahore Pakistan. Milli-Q water was used throughout experiments.

## 2.2. Green Synthesis of Iron Nanoparticle

The leaf extract from the plant *Terminalia chebula* was prepared through maceration, which was performed using 20 g of leaf powder with water as solvent (200 mL) at room temperature ( $28 \pm 2$  °C), with occasional shaking, for appx. 4 days. The extract was filtered and centrifuged to remove the debris. The supernatant obtained was preserved at temperature (4 °C). A solution of 0.1 M FeCl<sub>3</sub> was added to the leaf extract in a 2:3 volume ratio. The pH of solution was modified from 3 to 6 by adding 1.0 M NaOH. The formation of iron nanoparticles was indicated by the appearance of a black color precipitate, which was separated by centrifuging the solution at 7000 rpm for 15 min. The obtained black precipitate was washed and freeze-dried at  $-40$  °C at 10 Pa pressure for 24 h. The as-obtained iron nanoparticles were stored in an airtight dry container for further characterization and use.

## 2.3. Stabilization of Plant-Synthesized IONPs

### 2.3.1. Preparation of IONP-Loaded Chitosan Nanocomposites (IONPs-C)

IONP-C nanocomposites were prepared according to procedure reported by Jiang et al. [49]. In order to obtain different loadings of nanoparticles, three different concentrations of plant-synthesized IONPs (0.1 g, 0.15 g and 0.3 g) were added to the chitosan emulsion along with shaking and sonication in order to obtain a homogeneous mixture. The obtained nanocomposites were thoroughly washed with distilled water until pH was neutralized and before use. The three different nanocomposites containing different concentrations of IONPs obtained were labeled as IONPs-C-0.1, IONPs-C-0.15, and IONPs-C-0.3.

### 2.3.2. Preparation of IONP-Loaded PVA-Alginate Nanocomposites (IONPs-PA)

IONP-PA nanocomposites were prepared through the addition of a known quantity of alginate and desired concentration of nanoparticles solution to PVA solution, as reported earlier [50]. Briefly, 12 g PVA was added to 72 mL of water and stirred well in a conical flask for 5 h at 80 °C, while 1 g alginate was added to 20 mL of water and stirred in a separate flask. After mixing both solutions in a beaker, solutions with varying concentration of nanoparticles were added and continuously stirred. The mixture was dropped into a solution containing 6% boric and 2% calcium chloride with the help of an injector to obtain beads of the nanocomposites. The nanocomposites obtained were retained in the solution for the next 24 h and washed with distilled water several times for further use. The three different nanocomposites containing different concentrations of IONPs obtained were labeled as IONPs-PA-0.1, IONPs-PA-0.15, and IONPs-PA-0.3.

## 2.4. Material Characterization

The characterization studies were performed to analyze the physicochemical properties of the prepared samples. A UV-Visible spectrophotometer (UV-1800; Shimadzu, Tokyo, Japan) was used to measure the absorption spectra of IONPs synthesized by plant extract. For determination of the size of the IONPs and the morphological features of synthesized products, they were studied using a cold-field emission scanning electron microscope (CFE-SEM SU8200, Hitachi, Tokyo, Japan) equipped with energy-dispersive X-ray (EDX) spectroscopy. The amorphous/crystalline nature of the synthesized product was analyzed through X-ray powder diffraction (XRD) (Bruker D8 Advance, Karlsruhe, Germany) patterns using a Cu K $\alpha$  radiation ( $\lambda = 1.54$  Å) source. XRD patterns of the synthesized materials were analyzed in the range of  $2\theta$  from 20–80°. Malvern ZetaSizer (Malvern Instruments Ltd., Malvern, UK) was used to measure particle size/size distributions and zeta potential of plant-synthesized IONPs. Furthermore, the phytochemical composition of plant-synthesized iron nanoparticles was analyzed using a Fourier transform infrared (FTIR) spectrometer (Perkin

Elmer, Spectrum 400, Waltham, MA, USA) equipped with an attenuated total reflection (ATR) attachment (in a wave number ranging from 4000–650  $\text{cm}^{-1}$  by applying 20 scans at a resolution of 4  $\text{cm}^{-1}$ ). The Thermo Scientific™ K-Alpha+™ X-ray Photoelectron Spectrometer (XPS) System (Thermo Fisher Scientific, Waltham, MA, USA) was used to study the near-surface elemental composition of plant-synthesized IONPs.

### 2.5. Batch Adsorption Experiment for As(V) Removal

In this study, the plant-synthesized IONPs, IONPs–C, and IONPs–PA were used as adsorbents for the removal of As(V). A batch adsorption experiment was conducted with an aqueous solution of As(V). The experiments were carried out by shaking the aqueous solution of As(V) and adsorbents at 24 °C; the continuously shaking (120–125 rpm) was carried out to ensure a good contact of the nanocomposites with arsenic ions. The effect of various parameters on adsorption capacity were investigated, including pH, adsorbent dose, initial As(V) concentration, and contact time on removal of As(V) from solution. As(V) concentrations in aqueous samples before and after the experiments were measured by ICP-OES with 2%  $\text{HNO}_3$  digestion. All the experiments were performed in triplicates. The percentage of removal of arsenate was calculated with the following formula:

$$\% \text{ removal} = \frac{C_i - C_f}{C_i} \times 100, \quad (1)$$

where  $C_i$  and  $C_f$  are the initial concentration and final concentrations of the metal ion arsenic mg/L (present in sample), respectively.

The effect of the adsorbent dosage (0.05–0.5 g/L) and varying initial arsenic concentrations (1–50 mg/L) were investigated around  $\text{pH } 6.6 \pm 0.3$ . The influence of IONPs loading in the chitosan and PVA–alginate nanocomposites for removal of As(V) was also determined.

In order to investigate the effect of pH on adsorption, the pH varied from 2 to 10 with varying concentrations of arsenate, while keeping the adsorbents constant, i.e., 0.2 g/L IONP–C and IONP–PA nanocomposites loaded with 0.15 g IONPs were used to investigate the effect of pH on As(V) removal.

#### 2.5.1. Adsorption Kinetics

The adsorption kinetics of the prepared nanocomposites were performed at various initial concentrations of As(V) as a function of contact time. The experiments were carried out by placing 0.2 g/L of adsorbents in different conical flasks containing As(V) solution at  $\text{pH} = 6 \pm 0.4$ , agitated at 122 rpm at constant temperature ( $24.0 \pm 1$  °C). Samples were withdrawn for analysis at different intervals of time (0.5–6 h). The adsorption capacity of As(V) on the IONPs, IONPs–C, and IONPs–PA nanocomposites loaded with 0.15 g of IONPs were investigated.

#### 2.5.2. Adsorption Isotherm

Isotherm studies were conducted at different initial concentrations of arsenic (1–50 mg/L) with a constant weight of all three adsorbents (0.2 g/L) at  $\text{pH } 6 \pm 0.4$ . The equilibrium adsorption capacity ( $q_e$ ) was calculated from the below given formula:

$$q_e = \frac{C_i - C_e}{m} \times V, \quad (2)$$

where  $q_e$  represents adsorption capacity (mg/g).  $C_i$  and  $C_e$  are the initial concentration and equilibrium concentrations of the metal ion arsenic mg/L, respectively.  $V$  is the volume of arsenic solution (L), and  $m$  is the mass of adsorbent (g).

### 2.6. Reuse of Adsorbents and Iron Ion Release Study

The reusability of the iron nanoparticles, chitosan, and PVA–alginate nanocomposites was evaluated using repeated sorption–desorption cycles. Sorption experiments were performed using

a 0.5 g/L dosage of adsorbents with a concentration of As(V) 20 mg/L at pH  $6.4 \pm 0.2$ , 122 rpm at temperature 24 °C, while 50 mL of 0.1 M NaOH, was used as a desorbing agent. Three adsorbents loaded with arsenic metals were agitated separately in 0.1 M NaOH solution for 60 min. After each desorption process, the nanocomposites were washed with water until the pH of the solution obtained from the wash possessed a neutral pH, and then it was further reused for sorption studies. The arsenic concentration in adsorbed and desorbed solution was measured.

The release of iron ions from three adsorbents was also measured after each adsorption cycle. In addition, two separate experiments were performed to estimate the iron release from three adsorbents. Two doses of IONPs, 0.01 g/L and 0.5 g/L, were administered, while a single dose (0.5 g/L) of IONP-C and IONP-PA nanocomposites was used for 20 mg/L of As(V) solution. Samples were shaken continuously, and small aliquots were taken after different intervals of time for the testing of iron ions. Ions concentration in samples was measured by ICP-OES with 2% HNO<sub>3</sub> digestion.

### 3. Results and Discussion

#### 3.1. Characterization of Iron–Oxide Nanoparticles (IONPs)

Upon addition of ferric chloride solution to the aqueous leaf extract solution of *T. chebula*, the mixture rapidly turned from a light brown to dark black color, indicating the formation of IONPs, which was monitored/confirmed by UV-Vis spectroscopy as shown in Figure 1. UV analysis of ferric chloride solution displays two characteristic absorption bands at 270 nm and 378 nm; however, upon being treated with *T. chebula* extracts, the absorption bands were found to shift to 327 nm and 438 nm due to surface plasmon, which signifies the conversion of ferric chloride solution as an iron precursor to IONPs. It also signifies that the leaf extract acts as a reducing agent and may cause the reduction of the iron. The results are in agreement with studies carried out by other researchers reported in literature [51,52] and the little variation of peaks might be due to the presence of different phytochemicals in the plant material.

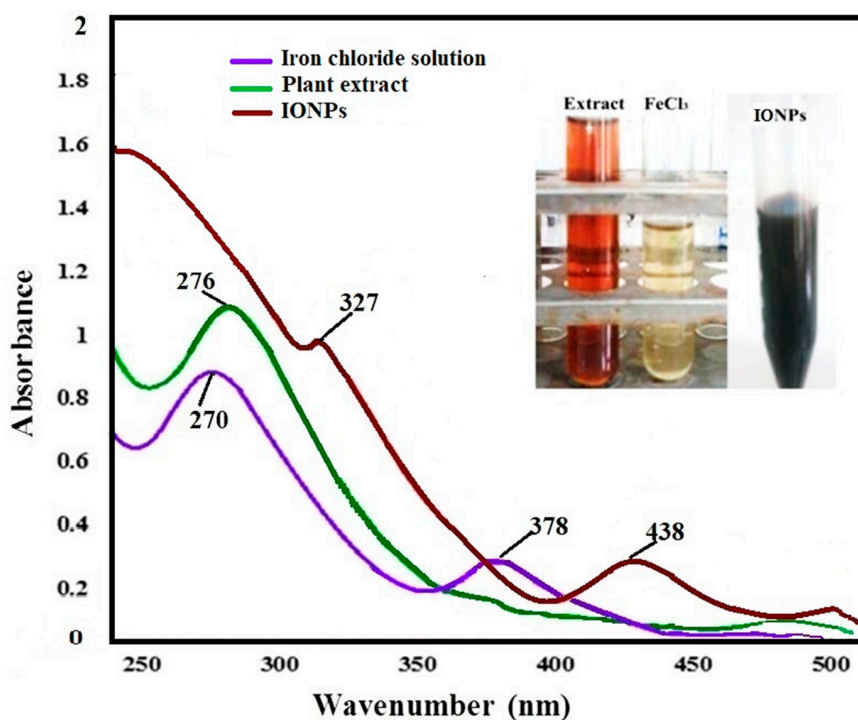
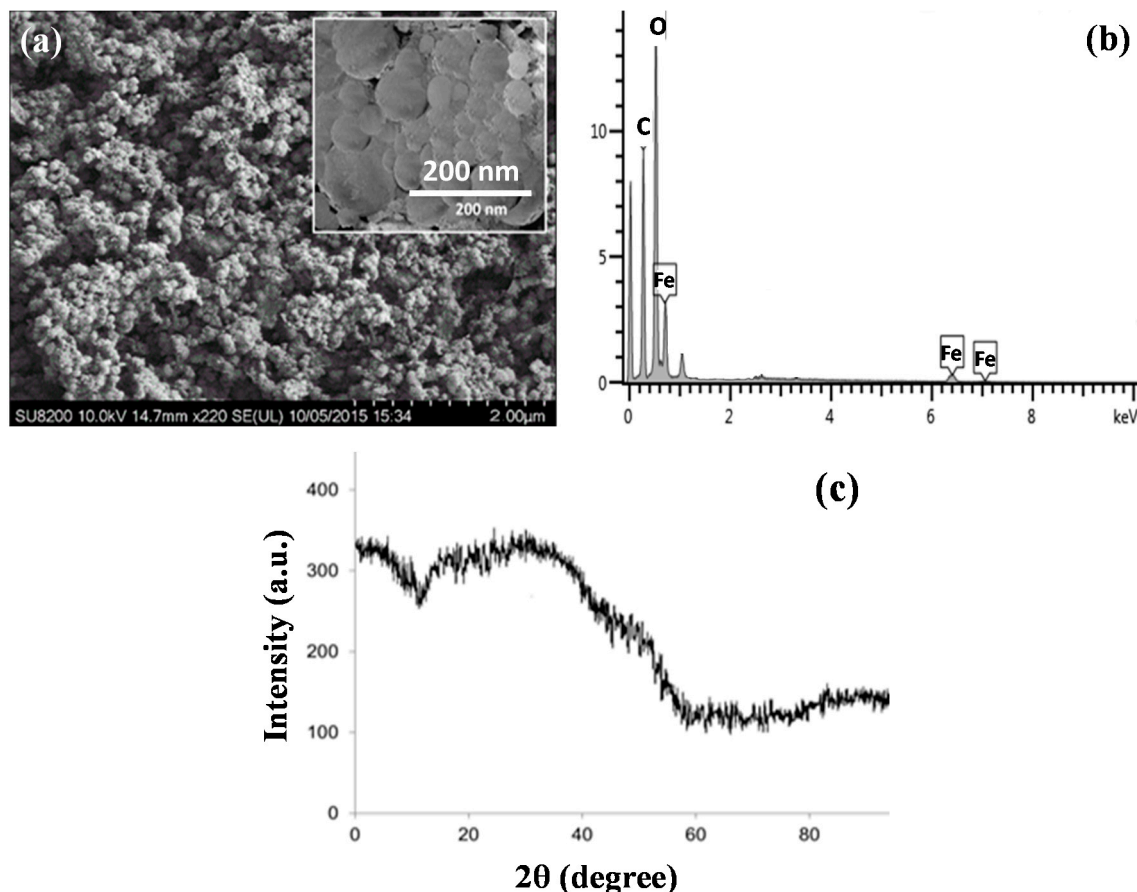


Figure 1. UV-Vis spectra of *Terminalia chebula*-employed iron–oxide nanoparticles (IONPs).

Scanning electron microscope images showed that IONPs formed are round in shape with less discrete particles, and the size is less than 100 nm (Figure 2a). An EDX spectrum of IONPs is shown in



Figure 2b. The EDX spectrum contains intense signals corresponding to Fe, O, and C. The C signals are attributed mainly to the polyphenol groups and other C-containing molecules in the extracts. The result of an EDX study was compared with the studies reported by other researchers [34,45], which corroborated the presence of carbon (C) on the surface of the green synthesized nanoparticles, which was further confirmed through X-ray diffraction spectroscopy.



**Figure 2.** (a) SEM images of *T. chebula*-synthesized IONPs and (b) EDX profile of IONPs. (c) XRD pattern of *T. chebula*-synthesized IONPs.

The XRD pattern of synthesized material is shown in Figure 2c. The less distinctive diffraction pattern obtained indicates that synthesized iron nanoparticles are amorphous in nature, while the broad bump around  $20^\circ$  to  $30^\circ$   $2\theta$  could be due to carbon-containing biomolecules from the leaf extract. The XRD pattern obtained was found to be in agreement with the XRD patterns of iron nanoparticles synthesized by *T. chebula* fruit extract [53], eucalyptus [35,54] and grape leaf extract [38].

Dynamic light scattering techniques were used for the determination of size/size distribution and zeta potential. The average zeta size of IONPs was found to be  $81.2 \pm 1.3$  nm and the maximum distribution was found below the 100 nm scale (Supplementary information Figure S1a). The zeta potential of *T. chebula*-synthesized nanoparticles was found to be  $-34.4 \pm 0.88$  mV (Supplementary information Figure S1b).

X-ray photoelectron spectroscopy (XPS) was used in order to confirm the oxidation state of Fe in prepared nanoparticles and surface elemental composition. Elemental analysis, which confirmed the presence of Fe, C, and O elemental signatures, is shown in Figure 3. The photoelectron peaks at 711.4 and 725 eV are the characteristic doublets of Fe 2p<sub>3/2</sub> and Fe 2p<sub>1/2</sub> core-level spectra of iron oxide, respectively. The peak binding energy at 533.2 eV is attributed to O1s. The XPS spectrum of iron-containing nanoparticles from *T. chebula* confirmed the presence of tri- and divalent iron atoms in the nanoparticles. The ratio of  $\text{Fe}^{(\text{II})}/\text{Fe}_{(\text{total})}$  and  $\text{Fe}^{(\text{III})}/\text{Fe}_{(\text{total})}$  was calculated by the peak area in the

core level spectra of Fe 2p and found to be 0.53 for Fe(III) and 0.46 for Fe(II). Thus, particles formed by *T. chebula* aqueous extract represent iron oxide (II, III) nanoparticles.

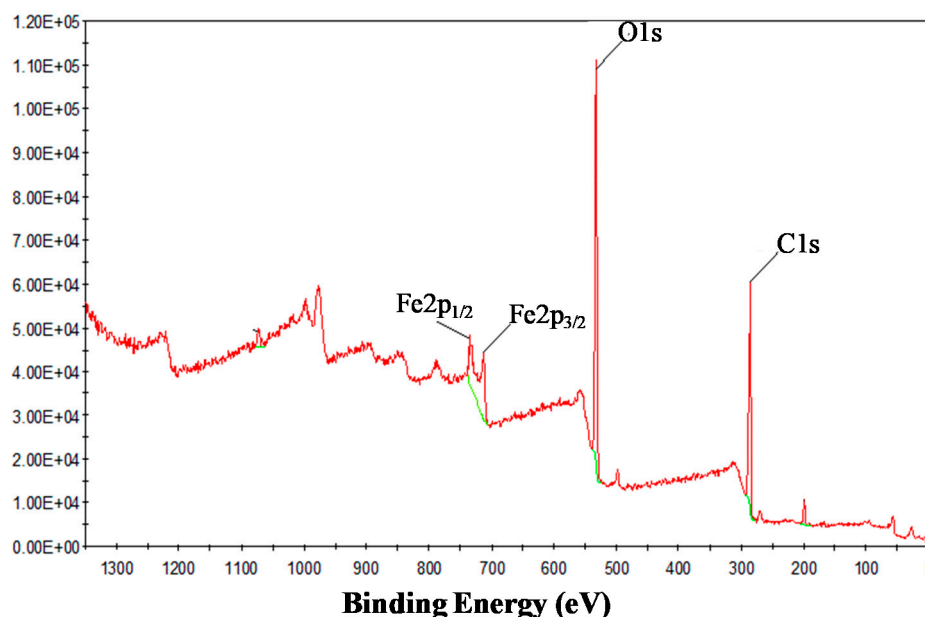


**Figure 3.** X-ray photoelectron spectroscopy (XPS) profile of IONPs synthesized by *T. chebula*.

In Figure 4a, the FTIR spectrum of the leaf extract of *T. chebula* gives information about the possible biomolecules present in the aqueous extract. There was a sharp peak in the phenolic region at  $3332\text{ cm}^{-1}$ ; however, two sharp peaks at  $2816\text{ cm}^{-1}$  and  $2793\text{ cm}^{-1}$  corresponded to a strong stretching vibration of the OH group of carboxylic acid and the alkyl group with medium bonding, which reveals the presence of significant polyphenols groups in *T. chebula* aqueous extract. Many peaks between the regions of 700 and  $1700\text{ cm}^{-1}$  were observed. The absorption peak around  $1593\text{ cm}^{-1}$  corresponded to aromatic bending of the alkene (C=C) group, while the peaks at 1457, 1268, and  $1138\text{ cm}^{-1}$  were due to the bending vibration of the  $\text{CH}_2$  group. The sharp absorption peak at  $1034\text{ cm}^{-1}$  was assigned to stretching vibration of primary alcohol (OH).

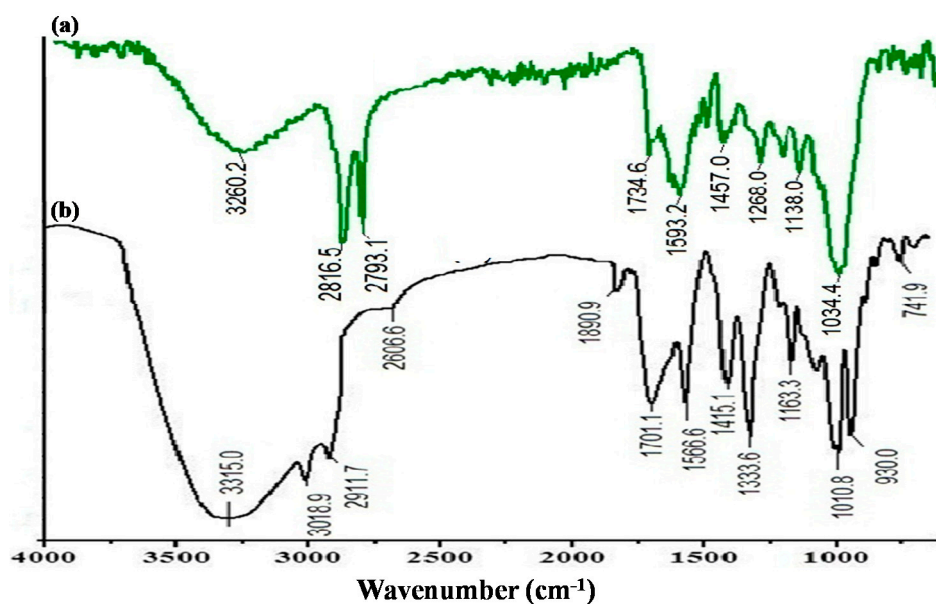


**Figure 4.** FTIR spectra of (a) *T. chebula* extract and (b) IONPs prepared employing *T. chebula* extract.

The polyphenols present in extract make complexes with iron metal ions and cling to metal [45]. Moreover, alcoholic functional groups (-OH) might be involved in the reduction as well as stabilization of the nanoparticles. The FTIR study revealed the interaction sites of extract molecules with iron metal ion to form IONPs. The FTIR spectra of *T. chebula*-synthesized IONPs showed several peaks in the spectral range of 700–3400  $\text{cm}^{-1}$ , indicating the presence of the phytomolecules from the extract on the surface of IONPs, which confirms the stabilizing role played by the phytomolecules in the synthesis of IONPs (Figure 4b). The sharp broad peak at 3315.0  $\text{cm}^{-1}$  was attributed to (O–H) phenols present at the surface of IONPs. Minor peaks at 3018  $\text{cm}^{-1}$ , 2911  $\text{cm}^{-1}$ , and 2606  $\text{cm}^{-1}$  were due to carboxylic acid and weak stretching of the alkyl group. The smaller feature band around 1890  $\text{cm}^{-1}$  was assigned to the bridged form of any alcoholic group (C=O) [55]. IR absorption peaks at 1701  $\text{cm}^{-1}$  and 1566  $\text{cm}^{-1}$  were attributed to the stretching of aldehydes (C=O) and bending of the medium aromatic (C=C) bond. A sharp peak at 1333  $\text{cm}^{-1}$  was assigned to the (C–N) amide; moreover, the peaks at 1163  $\text{cm}^{-1}$  and 1010  $\text{cm}^{-1}$  corresponded to the stretching vibration of the C–O bond, and the peak at 930  $\text{cm}^{-1}$  could be due to bending of the C–H alkane group.

### 3.2. FESEM and FTIR Study of Polymer-Supported IONPs

The SEM image of the IONPs–chitosan bead indicates the porous surface of chitosan surfaces, as shown in Figure 5a. Similarly, the morphology of IONP–PVA–alginate surfaces is clearly seen in Figure 5b. SEM images show that the polymer structures are crosslinked and have a compact uniform microstructure in nanocomposites (for more SEM images with different magnifications, see supplementary information Figure S2).

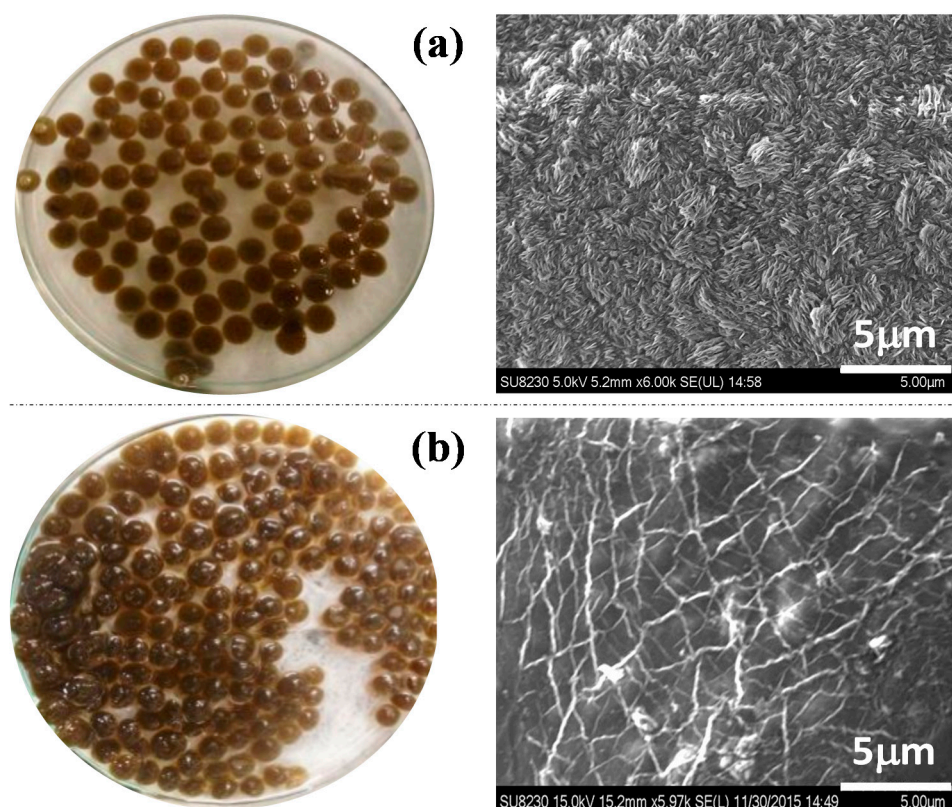


**Figure 5.** (a) IONP–C nanocomposites on different magnifications. (b) IONP–PA (polyvinyl alcohol (PVA)–alginate) nanocomposites surfaces at different magnifications.

FTIR spectroscopy was used to investigate the surface functional groups of IONPs–C, i.e., iron nanoparticles loaded to chitosan and IONP–PAs loaded to PVA–alginate (see supplementary



information Figure S3). The FTIR spectra of IONP–C and IONP–PA nanocomposites and arsenic adsorbed on IONP–C and IONP–PA nanocomposites are also given in Figure S4.

### 3.3. Arsenic Adsorption Results

#### 3.3.1. Effect of Nanoparticles Dosage and Initial Concentration on As(V) Removal

The effect of adsorbent dosages for the adsorption of As(V) from water was studied at pH  $6.6 \pm 0.3$ . The amount of plant-synthesized IONPs employed varied between 0.05–0.5 g/L, while the initial arsenic concentration varied from 1–50 mg/L; results are shown in Figure 6. It was observed that arsenic removal increased from 52% to 85% with an increase of the adsorbent dose from 0.05 g/L to 0.5 g/L at initial As(V) value of 1 mg/L. Thus, it can be concluded that the adsorbent dosage is an important factor to get the best results for pollutant removal.

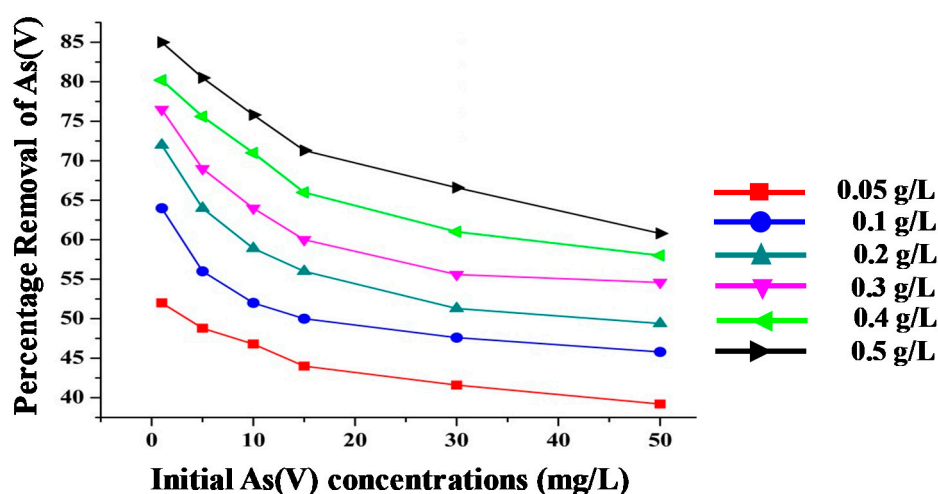


**Figure 6.** Effect of different doses of *T. chebula*-synthesized IONPs on removal of As(V) at different concentrations of As(V).

#### 3.3.2. Effect of IONPs Loading on Chitosan (IONPs–C) and PVA–alginate (IONPs–PA) Nanocomposites for As(V) Removal

To determine the effect of plant-synthesized IONPs loading to chitosan and PVA–alginate, i.e., IONPs–C and IONPs–PA, respectively, for removal of As(V), the nanocomposites containing varying amounts of IONPs (IONPs–C-0.1, IONPs–C-0.15, IONPs–C-0.3 and IONPs–PA-0.1, IONPs–PA-0.15, IONPs–PA-0.3) were used. Graphical illustrations of the results obtained for % removal of As(V) by IONPs loaded on polymer support at different As(V) concentrations are given in Figure 7. The results obtained showed that varying the amount of IONPs in the chitosan nanocomposites, i.e., IONPs–C-0.1, IONPs–C-0.15, and IONPs–C-0.3, has a prominent effect on the removed arsenic (72%, 88.6%, and 82.4% from 1 mg/L solution of arsenic, respectively), which reveals that initially increasing the load of IONPs from 0.1 g to 0.15 g in the chitosan nanocomposites improves the adsorption capacity, but further increasing from 0.15 g to 0.3 g results in a reduction in the adsorption capacities of the nanocomposites, which may be due to the availability of fewer adsorption active sites on the chitosan surface due to the increase of IONPs.

However, in the case of IONPs–PA, the adsorption of As(V) was increased from 66% to 82% when the IONP loading was increased from 0.1 g to 0.3 g, i.e., IONPs–PA-0.1, IONPs–PA-0.15, and IONPs–PA-0.3. It was also observed that the As(V) removal efficiency of polymer-supported IONPs (i.e., IONPs–C and IONPs–PA) is much higher than the As(V) removal efficiency of IONPs alone. Furthermore, when the polymer supports were tested for similar studies without the presence of the nanoparticles, i.e., IONPs, it was found that they displayed an adsorption efficiency of ~30%, while

with the presence of nanoparticles, the adsorption efficiency improved significantly, displaying an adsorption efficiency of 90%, indicating the importance of the presence of nanoparticles.

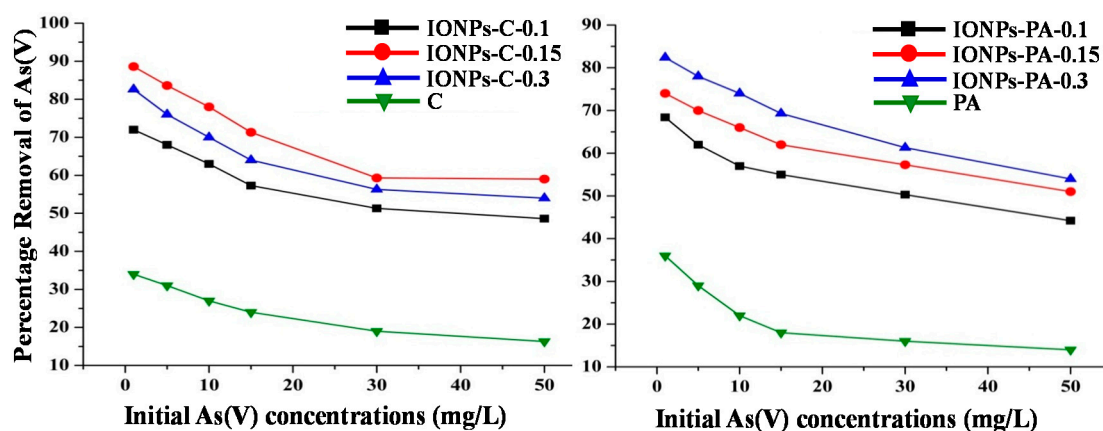


**Figure 7.** Effect of IONPs loading to chitosan nanocomposites (IONPs-C) and PVA-alginate nanocomposites (IONPs-PA) on removal of As(V).

### 3.3.3. Effect of pH and Initial Concentration on As(V) Removal

The adsorption efficiency of the IONPs and the nanocomposites, i.e., IONPs-C and IONPs-PA, for the removal of As(V) was studied by varying the pH of the solutions between 2–10, and the results are illustrated in Figure 8; Figure 9. Arsenate removal by IONPs was found to decrease from 98.9% to 82% when the pH varied from 2 to 10, when the solution of As(V) concentration was 1 mg/L (Figure 8). Results showed that the initial arsenic concentration as well as the pH influenced the adsorption capacity of the IONPs as well as of the composites; hence, the IONPs were subjected to the solution of an increasing concentration of As(V) from 1 mg/L to 50 mg/L, and the adsorption capacity of the IONPs decreased from 98.9% to 67% at pH 2. The adsorption efficiency of As(V) onto an iron surface was found to be dependent on pH, and the IONPs were found to be more effective at lower initial concentrations of arsenate in water. Similar trends have been reported in previous studies using various iron nanomaterials, and this has been well documented in other studies [9,56,57].

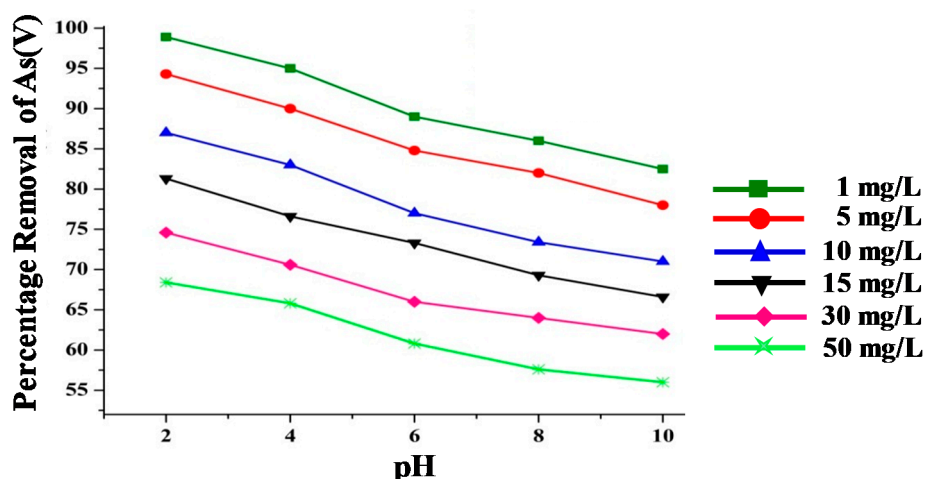


**Figure 8.** As(V) removal efficiency at different pH levels and arsenic concentration by IONPs.

Furthermore, the IONPs-C-0.15 and IONPs-PA-0.15 nanocomposites, i.e., chitosan nanocomposites and PVA-alginate nanocomposites with 0.15 g of IONPs, were selected for the study of their adsorption efficiency as a function of pH and initial arsenic concentration, and the results are illustrated in the Figure 9. The IONPs-C-0.15 was found to be effective at low pH for arsenic uptake from solution, which

was about 96.6% at pH < 3 (at initial 1 mg/L concentration of As(V)). The As(V) adsorption efficiency of the IONP–C-0.15 nanocomposites was found to reduce as the pH of the solution increased: At pH 8, the percentage removal was found to be about 82.5%; however, the adsorption efficiency was found to improve when the pH was further increased to 10 and the percentage removal was found to be 90%. Similar trends were found when the As(V) concentration in the solutions was increased.

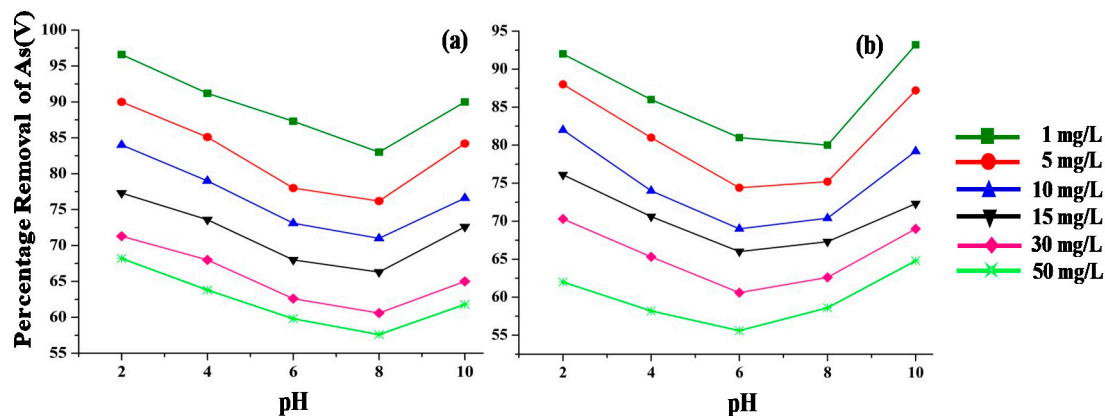


**Figure 9.** As(V) removal efficiency at different pH levels and arsenic concentration by (a) IONPs–C-0.15 and (b) IONPs–PA-0.15.

However, in the case of IONPs–PA-0.15, the PVA–alginate nanocomposites loaded with 0.15 g IONPs worked at both low and high pH levels but were more effective at high pH. A 91% to 93.2% removal of As(V) was noticed at pH = 3 and pH = 10, respectively, while a low adsorption trend was observed in the range of 6–8 pH, i.e., at initial 1 mg/L concentration of As(V). Moreover, IONPs–PA was found to be more effective at higher concentrations of arsenic compared to IONPs and IONPs–C at different pH levels.

### 3.3.4. Adsorption Kinetics

The adsorption capacity of As(V) on the IONPs and IONP–C, and IONP–PA nanocomposites in relation to time was investigated. Figure 10 shows the results for the amount adsorbed ' $q_t$ ' at time ' $t$ ' for the adsorbents. The As(V) solution concentration was varied by employing 5 mg/L, 10 mg/L, and 25 mg/L. No significant sorption took place with the passage of time by IONPs and IONP–C nanocomposites; however, for IONPs–PA, adsorption increased with time. Kinetic models pseudo-first-order and pseudo-second-order models were studied for these three adsorbents. The pseudo-first-order kinetic model equation is represented as:

$$\log(q_e - q_t) = \log q_e - \frac{K_1}{2.303} t, \quad (3)$$

where  $q_e$  and  $q_t$  are the amounts of As(V) adsorbed ( $\text{mg g}^{-1}$ ) at equilibrium time and at any instant of time,  $t$ , respectively, and  $K_1$  ( $\text{L min}^{-1}$ ) is the rate constant of the pseudo-first order sorption. This kinetics parameter was calculated by drawing the plot of  $\log(q_e - q_t)$  vs. ' $t$ '. The plot of  $\log(q_e - q_t)$  vs.  $t$  gave the straight lines with a slope of  $K_1$  and an intercept of  $\log q_e$  (Figure S4). The values of first order rate constants  $K_1$  and  $q_e$  were calculated from the slope and intercept of graphs and are given in Table 1.

The pseudo-second order model is represented by:

$$\frac{t}{q_t} = \frac{1}{K_2 q_e^2} + \frac{1}{q_e} t. \quad (4)$$

The values of  $K_2$  and  $q_e$  was calculated from the slope and intercept of plot of  $t/q_t$  versus  $t$  and are presented in Table 1. In this study, the correlation coefficients were examined for both kinetic

models. The low value of correlation coefficients ( $R^2 < 0.9$ ) was found in pseudo-first order kinetics and considered to be less favorable. However, in the pseudo-second-order model, the correlation coefficients of all examined data were found to be very high ( $R^2 \geq 0.99$ ).

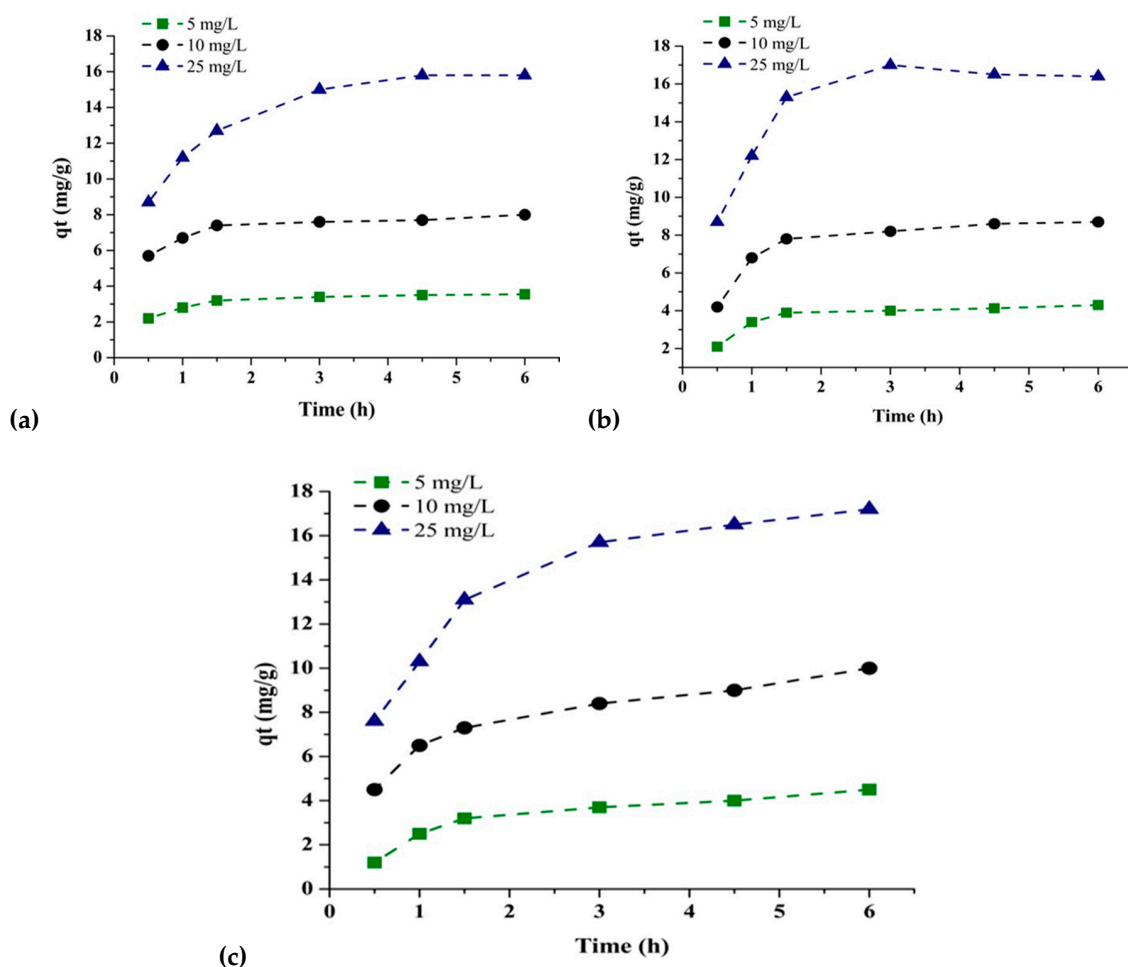


**Figure 10.** Arsenic removal efficiency at different time intervals and arsenic concentration by (a) IONPs (b), IONPs-C, and (c) IONPs-PA.

**Table 1.** Calculated parameters from pseudo-first model and pseudo-second order model of adsorption kinetics.

Adsorbents	Initial As (V) (mg/L)	Pseudo-First Order Model			Pseudo-Second Order Model		
		$K_1$ (min <sup>-1</sup> )	$q_e$ (mg g <sup>-1</sup> )	$R^2$	$K_2$ (mg g <sup>-1</sup> min <sup>-1</sup> )	$q_e$ (mg g <sup>-1</sup> )	$R^2$
IONPs	5	0.50	0.66	0.92	4.3	4	0.99
	10	0.4	0.75	0.86	3.8	8.3	0.99
	25	0.32	1.7	0.89	2.7	14.2	0.99
IONPs-C	5	0.581	1.15	0.98	2.38	4.62	0.99
	10	0.379	1.52	0.94	1.42	11.4	0.99
	25	0.11	2.4	0.81	1.33	19.2	0.99
IONPs-PA	5	0.62	0.67	0.99	0.9	5.10	0.99
	10	0.51	1.12	0.95	1.5	9.5	0.999
	25	0.138	1.7	0.97	1.1	21.2	0.99

### 3.3.5. Adsorption Isotherms

The correlation between the amount of arsenic adsorbed  $q_e$  (mg/g) and the arsenic concentration is presented by adsorption isotherms. The adsorption equilibrium isotherms Langmuir and Freundlich were used for the adsorption of arsenic(V) at neutral pH by IONPs and IONP-loaded chitosan and PVA-alginate nanocomposites where adsorbent dose 0.2 g/L was used.



A Langmuir adsorption isotherm was developed on the basis of an assumption that all the sites at the surface of the adsorbent are equivalent for adsorption to occur and also only monolayer formation could take place on the surface of the adsorbent. The isotherm was developed for gases and, hence, it is not that convenient to generalize it for the solution phase. However, an approximate model for liquid/solid interactions can be used to study the phenomenon of adsorption. The Langmuir isotherm does not account for the surface heterogeneity, and it does not take into account the adsorbate–adsorbate interactions and whether they are direct or indirect. It applies on completely homogeneous surfaces, i.e., maximum adsorption of the adsorbate occurs at homogeneous saturated monolayer sites on the adsorbent surfaces. The Langmuir adsorption isotherm can be represented by:

$$\frac{C_e}{q_e} = \frac{1}{q_m K_L} + \frac{C_e}{q_m}, \quad (5)$$

where  $C_e$  is As(V) ions equilibrium concentration in solution,  $q_e$  is the adsorption capacity based on the weight of the nanoadsorbent,  $q_m$  is the maximum amount of the As(V) adsorbed per unit mass of adsorbent to form a complete monolayer on the surface, and  $K_L$  is the Langmuir adsorption equilibrium constant (L/mg). The plot of  $C_e/q$  vs.  $C_e$  at various initial As(V) concentrations yielded straight lines, revealing that the adsorption of As ions follows the Langmuir adsorption equation (Figure S5). From the slope and intercept, the values of  $q_m$  and  $K$  for As(V) were calculated and are presented in Table 2. Maximum adsorption capacities ( $q_m$ ) of other adsorbents reported by literature are given in Table 3.

**Table 2.** Langmuir and Freundlich isotherms parameters for As(V) adsorption on different adsorbents.

Adsorbents	Langmuir Model		Freundlich Model	
	$q_m$ (mg/g)	$K_L$ (L/mg)	$1/n$	$K_f$ (mg/g)
IONPs	28.57	0.11	0.68	2.6
IONPs–C-0.1	27.7	0.088	0.64	3.17
IONPs–C-0.15	37.0	0.14	0.571	4.6
IONPs–C-0.3	34.48	0.05	0.76	1.84
IONPs–PA-0.1	33.2	0.07	0.78	2.06
IONPs–PA-0.15	37.03	0.06	0.76	2.3
IONPs–PA-0.3	40.3	0.1	0.64	3.8

The Freundlich isotherm was also applied for arsenic adsorption by adsorbents. This model relates to adsorption on heterogeneous surfaces with interaction between the adsorbed molecules. The well-known linear expression for the Freundlich model is given as:

$$\log q_e = \log K_f + \frac{1}{n} \log C_e, \quad (6)$$

where  $q_e$  is the amount adsorbed at equilibrium (mg/g),  $K_f$  is the Freundlich adsorption capacity parameter and  $1/n$  is the heterogeneity factor which is related to adsorption intensity, and  $C_e$  is the equilibrium concentration (mg/L). The values of  $1/n$  and  $K_f$  obtained from the slope and intercept of the plot of  $\log q_e$  against  $\log C_e$  and values are given in Table 2. The adsorption data of arsenic(V) removal by IONPs were fitted according to the linear form of the Langmuir adsorption. Arsenic removal by IONP–C and IONP–PA nanocomposites best fit the Freundlich model.

The Freundlich isotherm has one parameter,  $1/n$ , which indicates the surface heterogeneity and is used to describe the degree of curvature of the isotherms. As can be seen from Table 2, the values of  $n$  in all cases are greater than 1; therefore,  $1/n$  is less than 1. The variation of  $1/n$  ranging from 0 to 1 is associated to the chemisorption process, which tends to be more heterogeneous as the value gets close to zero [58]. For values greater than 0.7, it is implied that as the concentration of As(VI) increases, the relative adsorption decreases, indicating the saturation of adsorption sites.

**Table 3.** Adsorption capacity of different adsorbents for As(V) removal.

Type of Adsorbents	Adsorption Capacity ( $q_m$ )	Conditions	Ref.
Magnetic Fe <sub>2</sub> O <sub>3</sub> nanoparticles	88.44 mg/g at 10 °C, 95.37 mg/g at 20 °C, 105.25 mg/g at 30 °C	As = 10–200 mg/L, Adsorbent = 0.16 g, pH = 3	[17]
Zerovalent iron encapsulated chitosan nanospheres	119 ± 2.6 mg/g	As = 1–60 mg/L, Adsorbent = 0.1 g, pH = 7	[59]
Ascorbic acid-coated Fe <sub>3</sub> O <sub>4</sub> nanoparticles	16.56 mg/g	pH = 7, 300 K, 60 mg/L adsorbent	[60]
Starch and Carboxymethyl cellulose (CMC) zerovalent iron	14 mg/g	Adsorbent = 100–1000 mg/L, As = 2 mg/L, pH = 7	[61]
Zero valent iron reduced graphene	29.04 mg/g	10 mg adsorbent, As(V) = 1–15 ppm, pH = 7.0	[62]
Montmorillonite-supported nanoscale zero-valent iron	45.5 mg/g	As = 5–250 mg/L, Adsorbent = 1 g/L, pH = 7	[63]
Chitosan nanocomposites–magnetic nanoparticles	35.7 mg/g	Adsorbent = 1 g/L, pH = 6.8	[24]
Plant-synthesized IONPs chitosan hybrid	147 ± 7 mg/g	As(V) = 300–8000 µg/L, Adsorbent = 25 g/L	[64]

There is a certain correlation between the maximum sorption capacity and the percentage removal. Observing Table 2 and comparing it with Figures 6 and 7, it can be seen that IONPs–C-0.15 has the highest  $q_m$  (mg/g) and the same adsorbent shows the highest value of percentage removal seen from Figure 7. Therefore, it can be concluded that the best adsorption properties in terms of removal are depicted by IONPs–C-0.15 when we compare it with other chitosan loadings. Similarly, when we examine Figure 7 for IONPs–PA, it can be inferred that IONPs–PA-0.3 shows the highest percent removal of arsenic (V), which corresponds to the highest value of  $q_m$  (mg/g) given in Table 2 for the same adsorbent. Comparing Figure 6 and the values given in Table 2, it is observed that the polymer-loaded IONPs are better for removal of As(VI) than IONPs alone.

Upon comparison of the adsorption capacities of various other materials reported in literature (Table 3), it can be observed that the adsorption capacities are better than the material reported herein (Table 2). This could be explained by the fact that different adsorbents have different types of active sites. The number of active sites may also vary depending upon the nature of adsorbent, the method of its preparation, the temperature, and the pH.

### 3.4. Reuse of Adsorbent and Iron Ion Release

The reusability of IONPs and IONP–C, and IONP–PA nanocomposites using consecutive sorption–desorption cycles was evaluated, and the graphical representation of the results obtained is given in Figures 10 and 11. The adsorbent capacity decreased with the increasing number of cycles of reuse for all adsorbents prepared. However, in the case where IONPs were employed, the decrease in adsorbent capacity was prominent, which may be attributed to the higher affinity between the nanoparticles (adsorbent) and adsorbate, which is difficult to desorb [23], leading to the reduction in the number of active sites available upon reuse. However, in the case of IONP-loaded chitosan and PVA–alginate nanocomposites, it was observed that initially, the adsorption and desorption for chitosan was high, but both processes decreased with the increasing number of cycles. In the initial sorption cycle, IONPs and chitosan nanocomposites loaded with IONPs were more efficient than the PVA–alginate nanocomposites loaded with IONPs for removal of As(V). However, PVA–alginate nanocomposites showed better adsorption and desorption until the end of the fifth cycle than the other adsorbents. This is clearly shown in Figures 11 and 12. Polyvinyl alcohol (PVA) showed mechanical and chemical stability over other polymers and also possessed excellent adsorption capacity for the removal of toxic pollutants [50,65].

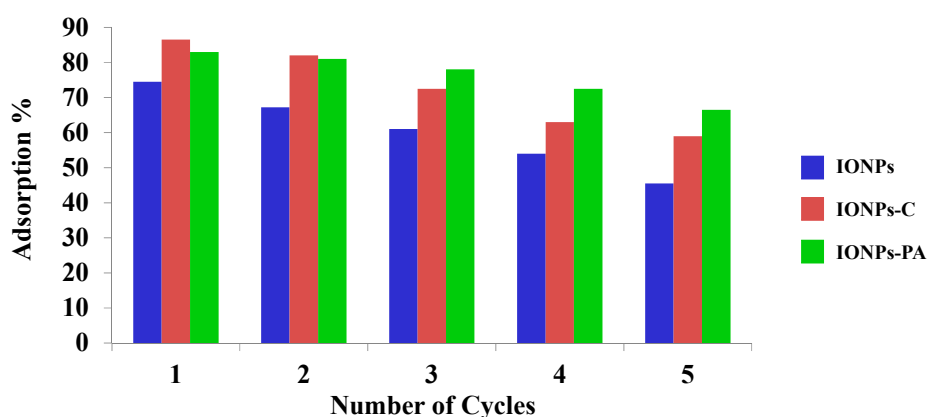
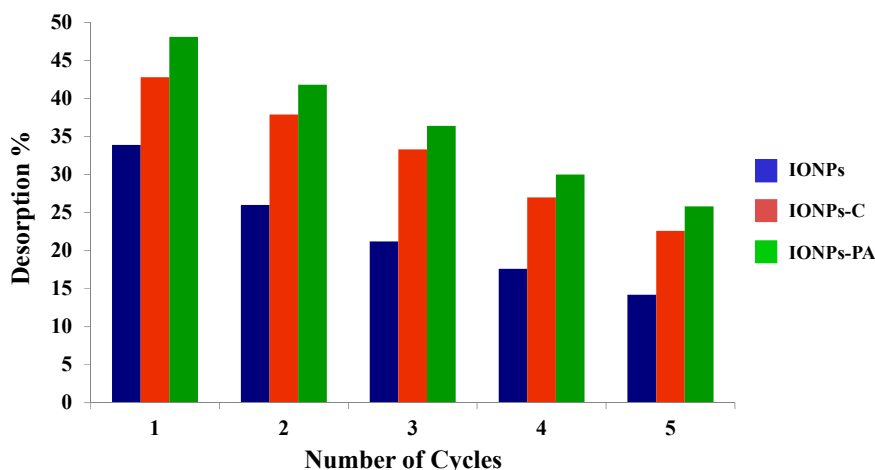


Figure 11. Adsorption cycles of adsorbents (IONPs; IONP-loaded chitosan and PVA–alginate nanocomposites).



**Figure 12.** Desorption cycles of adsorbents (IONPs; IONP-C and IONP-PA nanocomposites).

The dissolution of ions from metal oxide nanoparticles was considered an important factor, especially when accounting for nanoparticle toxicity. Therefore, in this study, ion release from nanoparticles was measured when the adsorbents are placed in an arsenic solution. After each adsorption cycle, the amount of iron was measured in an arsenic solution and results are given in Table 4. It was noticed that with the increasing number of cycles, the release of iron also increased from the adsorbents, i.e., iron nanoparticles and chitosan, but in the case of PVA–alginate nanocomposites, they contributed less to the release of ions in arsenic solution after five adsorption cycles. Hence, it can be concluded that consecutive sorption and desorption by alkaline media slowly degrades the polymers and becomes the cause of ion release from nanoparticles.

**Table 4.** Ion release from adsorbents after adsorption and desorption cycles (mg/L).

No. of Cycles	IONPs	IONPs-C-0.15	IONPs-PA-0.15
Cycle-1	0.06 ± 0.12	0.007 ± 0.2	0.002 ± 0.06
Cycle-2	0.14 ± 0.18	0.08 ± 0.21	0.026 ± 0.08
Cycle-3	0.28 ± 0.11	0.13 ± 0.13	0.051 ± 0.14
Cycle-4	0.4 ± 0.12	0.17 ± 0.11	0.078 ± 0.15
Cycle-5	0.54 ± 0.07	0.2 ± 0.20	0.12 ± 0.04

The experiment was repeated again to check the ion release from adsorbents; the iron ion release was noticed after different intervals of time in arsenic solution. Table 5 shows the profile of iron ion release from different iron adsorbents. The results indicate that IONPs without polymer support contribute to iron ion release, and the dissolution was increased by increasing the dose of nanoparticles in the solution. The ion release from chitosan and PVA–alginate was negligible even after 6 h. The study showed that the stability and reusability of PVA–alginate was much higher than that of the chitosan.

**Table 5.** Ion release from adsorbents at different time intervals (mg/L).

Time (h)	IONPs (0.01 g/L)	IONPs (0.5 g/L)	IONPs-C-0.15	IONPs-PA-0.15
0.5	0.00 ± 0.07	0.003 ± 0.07	0.00 ± 0.02	0.00 ± 0.06
1	0.006 ± 0.11	0.07 ± 0.11	0.008 ± 0.1	0.003 ± 0.12
2	0.02 ± 0.04	0.13 ± 0.04	0.03 ± 0.16	0.005 ± 0.14
4	0.05 ± 0.03	0.18 ± 0.22	0.04 ± 0.05	0.008 ± 0.22
6	0.08 ± 0.01	0.32 ± 0.14	0.07 ± 0.24	0.008 ± 0.06

#### 4. Conclusions

In this study, iron oxide nanoparticles (IONPs) were effectively synthesized by an aqueous leaf extract of *T. chebula* without using any hazardous reagents. Polymers such as chitosan and PVA–alginate



were used to stabilize nanoparticles and to obtain nanocomposites of the polymer–IONPs. To the best of our knowledge, this is the first study wherein green synthesized IONPs were stabilized using PVA–alginate polymer and chitosan and compared for their adsorption efficiency. The key findings are summarized as follows:

- i. A comparative adsorption study showed that the adsorption capacity of arsenate on IONPs and polymer-supported IONPs varied in different parameters, such as pH, initial concentration of arsenic, dosages of adsorbent, and contact time, and can be improved by changing these parameters.
- ii. Chitosan and PVA–alginate loaded with IONPs both were found to be more effective than the IONPs under different conditions of adsorption. The results also revealed that an increase of IONP loads to chitosan reduced the arsenic removal efficiency, but in the case of a PVA–alginate increase of IONPs, it increased the removal efficiency.
- iii. In solutions with lower concentrations of arsenic, the efficiency of the IONPs and IONP–C nanocomposites was found to be up to 99% and 96.6% at a pH below 3, respectively. Adsorption at low pH as well as at high pH was observed by IONP–PA nanocomposites, and their efficiency can be enhanced by increasing the contact time.
- iv. The adsorption kinetics was well fitted with a pseudo-second order reaction and the adsorption isotherm results were well-fitted with the Langmuir and Freundlich models.
- v. In the initial cycle, the sorption and desorption capacity of IONPs–C was remarkably high but decreased after a number of cycles. In the case of IONPs–PA, the reuse capacity was found to be more than that of the IONPs–C.
- vi. Results showed that ion release was negligible for polymeric stabilized iron nanoparticles, i.e., IONPs–C and IONPs–PA, even after cycle 5 (adsorption–desorption) compared to IONPs.

Our results indicated that the removal efficiency of As(V) by polymer-supported IONPs was higher than that of IONPs only. Hence, we state that our synthesized materials are more environmentally-friendly and cost-effective sorbents for arsenic removal from water. These findings reveal that the stabilized nanoparticles have great potential for in-situ and ex-situ remediation of arsenic. However, the improvement in reusability of the IONP-loaded polymer nanocomposites and the column study is to be further investigated in future.

**Supplementary Materials:** The following are included in <http://www.mdpi.com/2504-5377/3/1/17/s1>. Figure S1: (a) Zeta sizes and size distributions and (b) zeta potential of *T. chebula*-mediated IONPs. Figure S2: (a) Chitosan nanocomposites on different magnifications; (b) PVA–alginate nanocomposite surfaces at different magnifications. Figure S3: FTIR spectra of (a) IONP–C and (b) IONP–PA nanocomposites. Figure S4: FTIR spectra of (a) arsenic adsorbed IONP–C nanocomposites; (b) arsenic adsorbed on IONPs–PA nanocomposites. Figure S5: Pseudo-first order and pseudo-second order kinetics: (a) IONPs, (b) IONP–C nanocomposites, and (c) IONP–PA nanocomposites. Figure S6: Langmuir and Freundlich model: (a) IONPs, (b) IONP–C nanocomposites, and (c) IONP–PA nanocomposites.

**Author Contributions:** S.S. performed the related experiments and wrote the manuscript under the supervision of Y.C.; S.F.A. contributed towards writing and editing the manuscript. All authors have contributed, reviewed, and approved the final manuscript.

**Funding:** This research was partially supported by the U.S. National Science Foundation (NSF Grant no. CBET-1235166).

**Acknowledgments:** The authors acknowledge the Daniel Lab in School of Civil and Environmental Engineering and the Marcus Nanotechnology Research Center at Georgia Institute of Technology, Atlanta, USA.

**Conflicts of Interest:** The authors declare no conflict of interest.

## References

1. Khan, S.; Rauf, R.; Muhammad, S.; Qasim, M.; Din, I. Arsenic and heavy metals health risk assessment through drinking water consumption in the Peshawar District, Pakistan. *Hum. Ecol. Risk Assess.* **2016**, *22*, 581–596. [[CrossRef](#)]

2. Ali, Z.; Malik, R.N.; Qadir, A. Heavy metals distribution and risk assessment in soils affected by tannery effluents. *Chem. Ecol.* **2013**, *29*, 676–692. [[CrossRef](#)]
3. NRC. *Arsenic in Drinking Water*; National Academies Press: Washington, DC, USA, 2001.
4. Mostafa, M.; Cherry, N. Arsenic in Drinking Water, Transition Cell Cancer and Chronic Cystitis in Rural Bangladesh. *Int. J. Env. Res. Public Health* **2015**, *12*, 13739–13749. [[CrossRef](#)] [[PubMed](#)]
5. Oremland, R.S.; Stolz, J.F. The ecology of arsenic. *Science* **2003**, *300*, 939–944. [[CrossRef](#)] [[PubMed](#)]
6. Lee, Y.; Um, I.-h.; Yoon, J. Arsenic (III) oxidation by iron (VI)(ferrate) and subsequent removal of arsenic (V) by iron (III) coagulation. *Environ. Sci. Technol.* **2003**, *37*, 5750–5756. [[CrossRef](#)] [[PubMed](#)]
7. Hansen, H.K.; Ottosen, L.M. Removal of Arsenic from Wastewaters by Airlift Electrocoagulation: Part 3: Copper Smelter Wastewater Treatment. *Sep. Sci. Technol.* **2010**, *45*, 1326–1330. [[CrossRef](#)]
8. Genç-Fuhrman, H.; Tjell, J.C.; McConchie, D. Adsorption of Arsenic from Water Using Activated Neutralized Red Mud. *Environ. Sci. Technol.* **2004**, *38*, 2428–2434. [[CrossRef](#)]
9. Zhu, H.; Jia, Y.; Wu, X.; Wang, H. Removal of arsenic from water by supported nano zero-valent iron on activated carbon. *J. Hazard. Mater.* **2009**, *172*, 1591–1596. [[CrossRef](#)]
10. Reisner, D.E.; Pradeep, T. *Aquananotechnology: Global Prospects*; CRC Press: Boca Raton, FL, USA, 2014.
11. Cundy, A.B.; Hopkinson, L.; Whitby, R.L. Use of iron-based technologies in contaminated land and groundwater remediation: A review. *Sci. Total Environ.* **2008**, *400*, 42–51. [[CrossRef](#)]
12. Vilardi, G.; Mpouras, T.; Dermatas, D.; Verdone, N.; Polydera, A.; Di Palma, L. Nanomaterials application for heavy metals recovery from polluted water: The combination of nano zero-valent iron and carbon nanotubes. Competitive adsorption non-linear modeling. *Chemosphere* **2018**, *201*, 716–729. [[CrossRef](#)]
13. Xie, Y.; Fang, Z.; Qiu, X.; Tsang, E.P.; Liang, B. Comparisons of the reactivity, reusability and stability of four different zero-valent iron-based nanoparticles. *Chemosphere* **2014**, *108*, 433–436. [[CrossRef](#)] [[PubMed](#)]
14. Xiao, Z.; Yuan, M.; Yang, B.; Liu, Z.; Huang, J.; Sun, D. Plant-mediated synthesis of highly active iron nanoparticles for Cr(VI) removal: Investigation of the leading biomolecules. *Chemosphere* **2016**, *150*, 357–364. [[CrossRef](#)] [[PubMed](#)]
15. Biterna, M.; Arditoglou, A.; Tsikouras, E.; Voutsas, D. Arsenate removal by zero valent iron: Batch and column tests. *J. Hazard. Mater.* **2007**, *149*, 548–552. [[CrossRef](#)] [[PubMed](#)]
16. Tuutijärvi, T.; Lu, J.; Sillanpää, M.; Chen, G. As (V) adsorption on maghemite nanoparticles. *J. Hazard. Mater.* **2009**, *166*, 1415–1420. [[CrossRef](#)] [[PubMed](#)]
17. Lin, S.; Lu, D.; Liu, Z. Removal of arsenic contaminants with magnetic  $\gamma$ -Fe<sub>2</sub>O<sub>3</sub> nanoparticles. *Chem. Eng. J.* **2012**, *211*, 46–52. [[CrossRef](#)]
18. Wang, F.; Yang, W.; Zheng, F.; Sun, Y. Removal of Cr (VI) from simulated and leachate wastewaters by Bentonite-supported zero-valent iron nanoparticles. *Int. J. Env. Res. Public Health* **2018**, *15*, 2162. [[CrossRef](#)] [[PubMed](#)]
19. Yavuz, C.T.; Mayo, J.; William, W.Y.; Prakash, A.; Falkner, J.C.; Yean, S.; Cong, L.; Shipley, H.J.; Kan, A.; Tomson, M. Low-field magnetic separation of monodisperse Fe<sub>3</sub>O<sub>4</sub> nanocrystals. *Science* **2006**, *314*, 964–967. [[CrossRef](#)]
20. Badruddoza, A.Z.M.; Shawon, Z.B.Z.; Rahman, M.T.; Hao, K.W.; Hidajat, K.; Uddin, M.S. Ionically modified magnetic nanomaterials for arsenic and chromium removal from water. *Chem. Eng. J.* **2013**, *225*, 607–615. [[CrossRef](#)]
21. Gallios, G.; Tolkou, A.; Katsoyiannis, I.; Stefusova, K.; Vaclavikova, M.; Deliyanni, E. Adsorption of arsenate by nano scaled activated carbon modified by iron and manganese oxides. *Sustainability* **2017**, *9*, 1684. [[CrossRef](#)]
22. Mayo, J.; Yavuz, C.; Yean, S.; Cong, L.; Shipley, H.; Yu, W.; Falkner, J.; Kan, A.; Tomson, M.; Colvin, V. The effect of nanocrystalline magnetite size on arsenic removal. *Sci. Technol. Adv. Mater.* **2007**, *8*, 71–75. [[CrossRef](#)]
23. Yean, S.; Cong, L.; Yavuz, C.T.; Mayo, J.; Yu, W.; Kan, A.; Colvin, V.; Tomson, M. Effect of magnetite particle size on adsorption and desorption of arsenite and arsenate. *J. Mater. Res.* **2005**, *20*, 3255–3264. [[CrossRef](#)]
24. Wang, J.; Xu, W.; Chen, L.; Huang, X.; Liu, J. Preparation and evaluation of magnetic nanoparticles impregnated chitosan beads for arsenic removal from water. *Chem. Eng. J.* **2014**, *251*, 25–34. [[CrossRef](#)]
25. Krishnamurthy, S.; Frederick, R.M. Using biopolymers to remove heavy metals from soil and water. *Remediation* **1994**, *4*, 235–244. [[CrossRef](#)]

26. Gotoh, T.; Matsushima, K.; Kikuchi, K.-I. Preparation of alginate–chitosan hybrid gel beads and adsorption of divalent metal ions. *Chemosphere* **2004**, *55*, 135–140. [[CrossRef](#)] [[PubMed](#)]
27. Katsoyiannis, I.A.; Zouboulis, A.I. Removal of arsenic from contaminated water sources by sorption onto iron-oxide-coated polymeric materials. *Water Res.* **2002**, *36*, 5141–5155. [[CrossRef](#)]
28. Elwakeel, K.Z.; Guibal, E. Arsenic (V) sorption using chitosan/Cu (OH)<sub>2</sub> and chitosan/CuO composite sorbents. *Carbohydr. Polym.* **2015**, *134*, 190–204. [[CrossRef](#)] [[PubMed](#)]
29. Basu, H.; Singhal, R.; Pimple, M.; Reddy, A. Arsenic removal from groundwater by goethite impregnated calcium alginate beads. *Water Air Soil Pollut.* **2015**, *226*, 22. [[CrossRef](#)]
30. Singh, P.; Singh, S.K.; Bajpai, J.; Bajpai, A.K.; Shrivastava, R.B. Iron crosslinked alginate as novel nanosorbents for removal of arsenic ions and bacteriological contamination from water. *J. Mater. Res. Technol.* **2014**, *3*, 195–202. [[CrossRef](#)]
31. Rahimi, Z.; Zinatizadeh, A.; Zinadini, S. Membrane bioreactors troubleshooting through preparation of a high antifouling PVDF ultrafiltration mixed matrix membrane blended with O-carboxymethyl chitosan-Fe<sub>3</sub>O<sub>4</sub> nanoparticles. *Environ. Technol.* **2018**, 1–30. [[CrossRef](#)]
32. Woo, K.; Hong, J.; Choi, S.; Lee, H.-W.; Ahn, J.-P.; Kim, C.S.; Lee, S.W. Easy synthesis and magnetic properties of iron oxide nanoparticles. *Chem. Mater.* **2004**, *16*, 2814–2818. [[CrossRef](#)]
33. Chin, A.B.; Yaacob, I.I. Synthesis and characterization of magnetic iron oxide nanoparticles via w/o microemulsion and Massart's procedure. *J. Mater. Process Technol.* **2007**, *191*, 235–237. [[CrossRef](#)]
34. Shahwan, T.; Abu Sirriah, S.; Nairat, M.; Boyacı, E.; Eroğlu, A.E.; Scott, T.B.; Hallam, K.R. Green synthesis of iron nanoparticles and their application as a Fenton-like catalyst for the degradation of aqueous cationic and anionic dyes. *Chem. Eng. J.* **2011**, *172*, 258–266. [[CrossRef](#)]
35. Wang, Z. Iron Complex Nanoparticles Synthesized by Eucalyptus Leaves. *ACS Sustain Chem.* **2013**, *1*, 1551–1554. [[CrossRef](#)]
36. Prasad, K.S.; Gandhi, P.; Selvaraj, K. Synthesis of green nano iron particles (GnIP) and their application in adsorptive removal of As(III) and As(V) from aqueous solution. *Appl. Surf. Sci.* **2014**, *317*, 1052–1059. [[CrossRef](#)]
37. Pichsinee, S.; Karaked, T. Green synthesis of high dispersion and narrow size distribution of zero-valent iron nanoparticles using guava leaf (*Psidium guajava* L) extract. *Adv. Nat. Sci. Nanosci. Nanotech.* **2018**, *9*, 035006.
38. Luo, F.; Chen, Z.; Megharaj, M.; Naidu, R. Biomolecules in grape leaf extract involved in one-step synthesis of iron-based nanoparticles. *RSC Adv.* **2014**, *4*, 53467–53474. [[CrossRef](#)]
39. Smuleac, V.; Varma, R.; Sikdar, S.; Bhattacharyya, D. Green Synthesis of Fe and Fe/Pd Bimetallic Nanoparticles in Membranes for Reductive Degradation of Chlorinated Organics. *J. Memb. Sci.* **2011**, *379*, 131–137. [[CrossRef](#)]
40. Madhavi, V.; Prasad, T.N.; Reddy, A.V.; Ravindra Reddy, B.; Madhavi, G. Application of phyto-genic zerovalent iron nanoparticles in the adsorption of hexavalent chromium. *Spectrochim. Acta. A Mol. Biomol. Spectrosc.* **2013**, *116*, 17–25. [[CrossRef](#)]
41. Tandon, P.K.; Shukla, R.C.; Singh, S.B. Removal of arsenic(III) from water with clay-supported zerovalent iron nanoparticles synthesized with the help of tea liquor. *Ind. Eng. Chem. Res.* **2013**, *52*, 10052–10058. [[CrossRef](#)]
42. Kiruba Daniel, S.C.G.; Vinothini, G.; Subramanian, N.; Nehru, K.; Sivakumar, M. Biosynthesis of Cu, ZVI, and Ag nanoparticles using *Dodonaea viscosa* extract for antibacterial activity against human pathogens. *J. Nanopart. Res.* **2012**, *15*. [[CrossRef](#)]
43. Arokiyaraj, S.; Saravanan, M.; Udaya Prakash, N.K.; Valan Arasu, M.; Vijayakumar, B.; Vincent, S. Enhanced antibacterial activity of iron oxide magnetic nanoparticles treated with *Argemone mexicana* L. leaf extract: An in vitro study. *Mater. Res. Bull.* **2013**, *48*, 3323–3327. [[CrossRef](#)]
44. Kuang, Y.; Wang, Q.; Chen, Z.; Megharaj, M.; Naidu, R. Heterogeneous Fenton-like oxidation of monochlorobenzene using green synthesis of iron nanoparticles. *J. Colloid Interface Sci.* **2013**, *410*, 67–73. [[CrossRef](#)] [[PubMed](#)]
45. Wang, Z.; Fang, C.; Megharaj, M. Characterization of iron–polyphenol nanoparticles synthesized by three plant extracts and their Fenton oxidation of azo dye. *ACS Sustain Chem.* **2014**, *2*, 1022–1025. [[CrossRef](#)]
46. Wang; Lin, J.; Chen, Z.; Megharaj, M.; Naidu, R. Green synthesized iron nanoparticles by green tea and eucalyptus leaves extracts used for removal of nitrate in aqueous solution. *J. Clean. Product.* **2014**, *83*, 413–419. [[CrossRef](#)]
47. Han, Q.; Song, J.; Qiao, C.; Wong, L.; Xu, H. Preparative isolation of hydrolysable tannins chebulagic acid and chebulinic acid from *Terminalia chebula* by high-speed counter-current chromatography. *J. Sep. Sci.* **2006**, *29*, 1653–1657. [[CrossRef](#)] [[PubMed](#)]

48. Espenti, C.S.; Rao, K.K.; Rao, K.M. Bio-synthesis and characterization of silver nanoparticles using *Terminalia chebula* leaf extract and evaluation of its antimicrobial potential. *Mater. Lett.* **2016**, *174*, 129–133. [CrossRef]
49. Jiang, Y.-J.; Yu, X.-Y.; Luo, T.; Jia, Y.; Liu, J.-H.; Huang, X.-J.  $\gamma$ -Fe<sub>2</sub>O<sub>3</sub> nanoparticles encapsulated millimeter-sized magnetic chitosan beads for removal of Cr (VI) from water: Thermodynamics, kinetics, regeneration, and uptake mechanisms. *J. Chem. Eng. Data* **2013**, *58*, 3142–3149. [CrossRef]
50. Majidnia, Z.; Idris, A. Evaluation of cesium removal from radioactive waste water using maghemite PVA–alginate beads. *Chem. Eng. J.* **2015**, *262*, 372–382. [CrossRef]
51. Rosli, I.; Zulhaimi, H.; Ibrahim, S.; Gopinath, S.; Kasim, K.; Akmal, H.; Nuradibah, M.; Sam, T. Phytosynthesis of iron nanoparticle from *Averrhoa Bilimbi* Linn. In Proceedings of the IOP Conference Series: Materials Science and Engineering, Penang, Malaysia, 6–7 December 2017; p. 012012.
52. Mahdavi, M.; Namvar, F.; Ahmad, M.B.; Mohamad, R. Green biosynthesis and characterization of magnetic iron oxide (Fe<sub>3</sub>O<sub>4</sub>) nanoparticles using seaweed (*Sargassum muticum*) aqueous extract. *Molecules* **2013**, *18*, 5954–5964. [CrossRef]
53. Mohan Kumar, K.; Mandal, B.K.; Siva Kumar, K.; Sreedhara Reddy, P.; Sreedhar, B. Biobased green method to synthesise palladium and iron nanoparticles using *Terminalia chebula* aqueous extract. *Spectrochim. Acta. A Mol. Biomol. Spectrosc.* **2013**, *102*, 128–133. [CrossRef]
54. Wang; Jin, X.; Chen, Z.; Megharaj, M.; Naidu, R. Green synthesis of Fe nanoparticles using eucalyptus leaf extracts for treatment of eutrophic wastewater. *Sci. Total Environ.* **2014**, *466*, 210–213. [CrossRef] [PubMed]
55. Liu, Y.-T.; Yuan, Q.-B.; Duan, D.-H.; Zhang, Z.-L.; Hao, X.-G.; Wei, G.-Q.; Liu, S.-B. Electrochemical activity and stability of core–shell Fe<sub>2</sub>O<sub>3</sub>/Pt nanoparticles for methanol oxidation. *J. Power Sources* **2013**, *243*, 622–629. [CrossRef]
56. Stollenwerk, K.G. Geochemical Processes Controlling Transport of Arsenic in Groundwater: A Review of Adsorption. In *Arsenic in Ground Water*; Welch, A.H., Stollenwerk, K.G., Eds.; Springer: New York, NY, USA, 2003; p. 475.
57. Kanel, S.R.; Greneche, J.-M.; Choi, H. Arsenic (V) removal from groundwater using nano scale zero-valent iron as a colloidal reactive barrier material. *Environ. Sci. Technol.* **2006**, *40*, 2045–2050. [CrossRef] [PubMed]
58. Karnitz, O., Jr.; Gurgel, L.V.A.; De Melo, J.C.P.; Botaro, V.R.; Melo, T.M.S.; de Freitas Gil, R.P.; Gil, L.F. Adsorption of heavy metal ion from aqueous single metal solution by chemically modified sugarcane bagasse. *Bioresource Technol.* **2007**, *98*, 1291–1297. [CrossRef] [PubMed]
59. Gupta, A.; Yunus, M.; Sankaramakrishnan, N. Zerovalent iron encapsulated chitosan nanospheres—a novel adsorbent for the removal of total inorganic arsenic from aqueous systems. *Chemosphere* **2012**, *86*, 150–155. [CrossRef] [PubMed]
60. Feng, L.; Cao, M.; Ma, X.; Zhu, Y.; Hu, C. Superparamagnetic high-surface-area Fe<sub>3</sub>O<sub>4</sub> nanoparticles as adsorbents for arsenic removal. *J. Hazard. Mater.* **2012**, *217*, 439–446. [CrossRef] [PubMed]
61. Mosaferi, M.; Nemati, S.; Khataee, A.; Nasser, S.; Hashemi, A.A. Removal of Arsenic (III, V) from aqueous solution by nanoscale zero-valent iron stabilized with starch and carboxymethyl cellulose. *J. Environ. Health. Sci. Eng.* **2014**, *12*, 74. [CrossRef]
62. Wang, C.; Luo, H.; Zhang, Z.; Wu, Y.; Zhang, J.; Chen, S. Removal of As(III) and As(V) from aqueous solutions using nanoscale zero valent iron-reduced graphite oxide modified composites. *J. Hazard. Mater.* **2014**, *268*, 124–131. [CrossRef]
63. Bhowmick, S.; Chakraborty, S.; Mondal, P.; Van Renterghem, W.; Van den Berghe, S.; Roman-Ross, G.; Chatterjee, D.; Iglesias, M. Montmorillonite-supported nanoscale zero-valent iron for removal of arsenic from aqueous solution: Kinetics and mechanism. *Chem. Eng. J.* **2014**, *243*, 14–23. [CrossRef]
64. Martínez-Cabanas, M.; López-García, M.; Barriada, J.L.; Herrero, R.; Sastre de Vicente, M.E. Green synthesis of iron oxide nanoparticles. Development of magnetic hybrid materials for efficient As(V) removal. *Chem. Eng. J.* **2016**, *301*, 83–91. [CrossRef]
65. Chuan, L.T.; Manap, N.; Abdullah, H.Z.; Idris, M. Polyvinyl Alcohol-Alginate Adsorbent Beads for Chromium (VI) Removal. *Int. Eng. Technol.* **2018**, *7*, 95–99.

